

# Multi-orbital Anderson models and the Kondo effect: A post-NCA study

Norbert Grewe, Torben Jabben and Sebastian Schmitt

Institut für Festkörperphysik, Technische Universität Darmstadt, Hochschulstr. 6, D-64289 Darmstadt, Germany

Received: date / Revised version: date

**Abstract.** The low energy region of certain transition metal compounds reveals dramatic correlation effects between electrons, which can be studied by photoelectron spectroscopy. Theoretical investigations are often based on multi-orbital impurity models, which reveal modified versions of the Kondo effect. We present a systematic study of a multi-orbital Anderson-like model, based on a new semi-analytical impurity solver which goes beyond simple modifications of the well known NCA. We discuss one-particle excitation spectra and in particular the role of level positions and Coulomb-matrix elements. It is shown that the low-energy region as well as the overall features of spectra critically depend on the model parameters and on the quality of the approximations used. Recent photoelectron experiments and corresponding existing calculations are put into perspective. An interesting crossover scenario between different regimes of ground states with characteristically different local correlations is uncovered.

**PACS.** 71.10.-w Theories and models of many-electron systems – 71.20.-b Electron density of states and band structure of crystalline solids – 71.27.+a Strongly correlated electron systems; heavy fermions – 71.55.-i Impurity and defect levels

## 1 Introduction

The Anderson model with a spin-degenerate local level hybridized to a broad conduction band has served in studies of the Kondo effect [1–3] and, combined with approximations like DMFT, also in investigations of the behavior of lattice-periodic systems [4–6]. In connection with lattice systems it plays the role of an effective impurity which, as part of a self consisting cycle, has to be solved for the Greens functions of local electrons by use of appropriate impurity solvers. Among these impurity solvers are numerical ones like QMC [7, 8] or NRG [9, 10] and so called semi-analytical ones, which are based on direct perturbation theory with respect to hybridization and which rely on numerical procedures to solve implicit equations for propagators formulated via skeleton-diagram techniques [11–15]. The former essentially exact methods in fact can properly describe the low energy region of the model but are either limited to relatively small interaction values or high temperatures due to numerical obstacles and exhibit deficiencies for higher excitation energies. The newly developed semi analytical methods like ENCA, SUNCA, and CA1 [16–18], which improve the well known NCA [13, 19, 20, 14] via inclusion of vertex corrections with crossing diagrams, on the other hand are well suited for the whole range of excitation energies.

Capturing electron correlations due to strong local interactions in realistic transition metal compounds, in the framework of band structure theory or in form of quasi-

particle band structures derived from Greens functions, is an active field of research [21–23]. Difficulties arise from the effective local building blocks needed in the theories, which in most cases are more complicated than a simple Anderson impurity.

A connected problem of equal relevance arises in the interpretation of data from photoelectron spectroscopy (PES) in Ce-compounds, which hopefully can demonstrate the Kondo physics via direct observation of the formation of a many-body resonance near the Fermi level [24, 25]. Here it is the influence of crystal-field levels and spin-orbit splitting, possibly also of higher levels on Ce with double occupancy, which complicates the picture and greatly enhances the necessary numerical effort. Since the resolution of inverse PES still is not sufficiently high enough to measure directly all details needed of the DOS above the Fermi level  $\epsilon_F$ , one relies on direct PES together with extrapolations into a limited region of thermally occupied states above  $\epsilon_F$ . Although a consistent picture of the many-body effects in some of the Ce-compounds arises [26], some uncertainties remain. In particular, comprehensive and reliable information about the whole spectral region of energies up to the excitation energies of local states with differing occupancy and their influence on the low-energy region is highly desirable.

Attempts of calculating one-particle excitation spectra for multi-orbital atoms in a metallic host in the frame of direct perturbation theory have so far been based on the NCA as a theory designed for the case of infinite lo-

cal Coulomb repulsion  $U$  [26,27], with some simple adaptations for the additional orbitals [28,29]. Vertex corrections have thus been neglected and only two possibilities for the occupancy of the local shell are realized. Published attempts to improve on this kind of approach have not furnished e.g. improved excitation spectra yet [30]. Nevertheless, it is known, that even for the simple Anderson model important modifications arise from better approximations and more realistic values of the local Coulomb repulsion, concerning e.g. the characteristic low energy scales as well as the bulk of the more remote spectrum above the Fermi level [16].

A recent study [18] has demonstrated that among a few existing qualitative improvements of NCA, some of them with even somewhat higher accuracy, the ENCA can serve as a rather reliable approximation in a large region of excitation energies, and that the numerical effort is limited and can be handled well. ENCA goes considerably beyond NCA; it includes all vertex corrections up to second order in the hybridization strength and describes the region of all finite  $U$ . ENCA e.g. correctly reproduces the low energy scale  $T_K$  with its dependence on model parameters [16].

We have generalized the ENCA to the case of a multi-orbital model and present here a systematic study of this new ENCACF. We will discuss some interesting features arising from variations of shell energies and different local Coulomb-matrix elements. As it will turn out, consistent interpretations of many features of the spectra calculated are possible, revealing some interesting physical trends and hopefully enabling an improved understanding of measured spectra.

In the following section 2 we shortly present the model and the construction of our ENCACF approximation and we also compare some basic features with earlier approximations. Section 3 contains our main results in form of calculated series of spectra for varying model parameters and relevant physical interpretations. A summary and some remarks on future developments concludes our paper in section 4.

## 2 A multi-orbital Anderson model and the ENCACF approximation scheme

When setting up realistic models for transition metal atoms with open inner shells, one is confronted with the problem of dealing with several free parameters which, though in principle to be determined consistently from first principles, can usually not be fixed with sufficient accuracy. For definite host materials some information from experiments and from basic calculations like band structure theory is available and may help to define relevant regimes. In a situation, where physics is intricate and the validity of approximations is questionable, an approach via a somewhat restricted model seems appropriate. We therefore will study the following generalization of the well known

Anderson model:

$$\hat{H} = \sum_{j,\sigma} \left[ \epsilon_j \hat{n}_{j\sigma} + \sum_{\underline{k}} \epsilon_{j\underline{k}} \hat{n}_{j\underline{k}\sigma} + \frac{V_j}{\sqrt{N_0}} \sum_{\underline{k}} \left( \hat{c}_{j\underline{k}\sigma}^\dagger \hat{f}_{j\sigma} + \hat{f}_{j\sigma}^\dagger \hat{c}_{j\underline{k}\sigma} \right) \right] + \sum_j U_{jj} \hat{n}_{j\uparrow} \hat{n}_{j\downarrow} + \sum_{j<l} \sum_{\sigma,\sigma'} U_{jl} \hat{n}_{j\sigma} \hat{n}_{l\sigma'} \quad (1)$$

Here  $\hat{c}_{j\underline{k}\sigma}^\dagger$  creates an electron in band  $j$  with crystal momentum  $\underline{k}$ , spin  $\sigma$  and energy  $\epsilon_{j\underline{k}}$ ,  $\hat{f}_{j\sigma}^\dagger$  creates an electron in a local level  $j$  with spin  $\sigma$  and energy  $\epsilon_j$ , and  $\hat{n}_{j\sigma} = \hat{f}_{j\sigma}^\dagger \hat{f}_{j\sigma}$ ,  $\hat{n}_{j\underline{k}\sigma} = \hat{c}_{j\underline{k}\sigma}^\dagger \hat{c}_{j\underline{k}\sigma}$  are the corresponding occupation-number operators. The  $V_j$  denote (real) matrix elements for local hybridization between an electron in band  $j$  and one in a local level  $j$ , both with the same spin. Thereby we assume, as usual, that one-particle states can be classified according to their crystal symmetry with respect to the position of the impurity. With  $j$  being the relevant quantum number, hybridization in our model thus respects crystal and spin symmetry separately. Insofar as only the local hybridization intensities  $\Delta_j(\omega) = V_j^2 \rho_j^{(0)}(\omega)$ , with  $\rho_j^{(0)}(\omega) = \frac{1}{N_0} \sum_{\underline{k}} \delta(\omega - \epsilon_{j\underline{k}})$  being the DOS of band  $j$ , enter the following calculation, one may likewise speak of one single band and its respective symmetry components around the impurity.

From a formal point of view, as well as from the physics of the model, conservation of  $j$  is important for the proper implementation of our diagrammatic approach, i.e. in the identification of irreducible pieces. We comment in the conclusion on how this is to be changed when studying lattice systems or complexes with several centers. In general the local Coulomb matrix elements  $U_{jl}$  differ, depending on the states  $j$  and  $l$  involved.

Altogether the model (1) contains a whole set of parameters, including the functions  $\rho_j^{(0)}(\omega)$ . Unless one is able to derive all of these to a good accuracy with a specific situation in mind some reasonable assumptions have to be made in order to restrict the wealth of detailed information obtainable to some typically situations and trends. We therefore assume just two local levels  $\epsilon_1 \leq \epsilon_2$ , i.e.  $j = 1, 2$ , without further degeneracies besides spin, and also set the two band dispersions  $\epsilon_{1\underline{k}} = \epsilon_{2\underline{k}}$  equal, as well as the corresponding hybridization matrix elements  $V_1 = V_2$ . These are not completely unphysical assumptions; they can be realized in a highly symmetric situation, e.g. for  $p$ -states aligned along different axes of a cubic crystal.

For the transition metals we have in mind, the  $U_{jl}$  will typical be of the order of the bandwidth  $W$ , and  $U_{12}$  might be somewhat smaller than  $U_{11}$  and  $U_{22}$ . We will consider the cases  $U_{11} = U_{22} = U_{12} \equiv U$  and  $U_{11} = U_{22} = U$  with varying  $U_{12}$ .

Assuming a simple-cubic structure and a half-filled tight-binding band centered around the chemical potential at  $\epsilon_{\underline{k}} = \mu = 0$ , the unperturbed conduction band

DOS  $\rho^{(0)}(\omega)$  stretches from  $\omega = -3$  to  $\omega = 3$  with van-Hove kinks at  $\omega = \pm 1$ . We work with a fixed Anderson width  $\Delta \equiv \pi V^2 \rho^{(0)}(0) = 0.3 = W/20$ . Typically  $\epsilon_1 = -1$  lies in the occupied band region,  $U_{jl}$  exceeds  $|\epsilon_1|$ , and  $\epsilon_2$  varies between  $\epsilon_1$  and the upper band edge. Thus, a typical Kondo regime in the sense of the original Anderson model is studied.

The model (1) allows for a series of local occupation numbers, which in increasing order cause total shell energies elevated by one of the Coulomb energies  $U_{jl}$ . We restrict ourselves mostly to the three lowest values  $n_{loc} = 0, 1, 2$  by properly truncating the system of integral equations to be introduced below. This implies the following local shell-states with the corresponding energies:

$n_{loc}$	partial occupations	energy
0	$n_{1\sigma} = n_{2\sigma'} = 0$	$E_0 = 0$
1	$n_{1\sigma} = 1, n_{1-\sigma} = n_{2\sigma'} = 0$	$E_{1;1} = \epsilon_1$
1	$n_{2\sigma} = 1, n_{2-\sigma} = n_{1\sigma'} = 0$	$E_{1;2} = \epsilon_2$
2	$n_{1\sigma} = n_{1-\sigma} = 1, n_{2\sigma'} = 0$	$E_{2;11} = 2\epsilon_1 + U_{11}$
2	$n_{2\sigma} = n_{2-\sigma} = 1, n_{1\sigma'} = 0$	$E_{2;22} = 2\epsilon_2 + U_{22}$
2	$n_{1\sigma} = n_{2\sigma'} = 1$ $n_{1-\sigma} = n_{2-\sigma'} = 0$	$E_{2;12} = \epsilon_1 + \epsilon_2 + U_{12}$

The unperturbed one-particle excitation energies involve all possible differences between two of the above levels with difference one in the total local occupation number  $n_{loc}$ . This simple fact is useful to remember when interpreting calculated spectra in the next section. For a complete classification of the high energy region the scheme has to be extended to  $n_{loc} = 3$  and  $n_{loc} = 4$ . This should be kept in mind, when spectral weight has to be accounted for, which is missing from the calculation due to the neglect of the corresponding propagators.

The theoretical setup of semi analytical impurity solvers is based on the early work of Keiter and Kimball [11,31] and was brought into a form used today about 25 years ago [13,14,20]. It starts as "direct" time ordered perturbation theory in one-particle matrix elements between local and band states or in transfers between neighboring sites; Wick's theorem and Feynman diagrammatics cannot be used due to the presence of local interactions in the unperturbed Hamiltonian [12,32]. An alternative though equivalent approach uses additional, unphysical particles ("slave bosons") in order to stay in the frame of Feynman perturbation theory [33,34].

In either formulation skeleton-diagram techniques are used to perform the infinite summations, which are necessary to capture the essence of the many-body effects, i.e. the Kondo effect as a prototypical example, determining the ground state and low-lying excitations. The implicit equations for various types of propagators of local many body states, formulated via skeleton diagrams, constitute a system of singular complex integral equations, which apart from a few special simple cases have to be solved numerically. Since the perturbational setup and the particular diagram techniques are well documented [32,19,13,12,15], we will restrict our presentation to the new features and approximations developed for the multi-orbital model of equation (1). Various approximation schemes and relevant numerical techniques have recently been investi-

gated and compared, regarding their quality and validity, in applications to the Anderson model and to simple lattice models [18]. We will rely on the experience gathered there and will adopt the ENCA in a proper generalization to the multi-orbital situation. Direct perturbation theory involves the bonus of allowing a direct interpretation of diagrams in terms of physical processes [32,12]. Therefore we will present corresponding pictures in order to shortly explain the ideas behind the ENCACF used in the following calculations.

Propagators for states of the local shell evolve via excitation processes along a time axis with imaginary time for technical reasons. Pieces of processes, which are internally connected via lines visualizing excitations into the band, constitute irreducible self-energies for the propagators. The self-energy diagrams corresponding to a local state with just one electron of spin  $\sigma$  in orbital  $\epsilon_1$  are depicted in Fig. 1(a). The earliest, i.e. lowest band electron line, labeled  $(\underline{k}, \sigma')$ , determines via its direction, upward or downward, whether the following local state has zero or two electrons. In the first diagrammatic contribution it is the vacuum state  $|0\rangle$ , in the following two cases the hybridization event according to equation (1), is absorbed either in level  $\epsilon_1$  or in level  $\epsilon_2$ . Two electrons in level  $\epsilon_1$  are to have opposite spins, i.e.  $\sigma' = -\sigma$  here, while in the last contribution the second spin-direction  $\sigma'$  is free to be summed over as well as the crystal momentum  $\underline{k}$ . All later hybridization events can be collected in the vertex functions, represented by the different triangles for the three cases. Approximations to be made concern these vertex functions. In a simple non-crossing approximation, adopted to this multi-orbital case (SNCACF), the triangles are just replaced by bare vertices.

Although this scheme looks very simple, it is the use of full propagators for all local lines shown, with the self-energies under debate inserted, which already makes it highly non-trivial and allows e.g. for a qualitative description of Kondo physics. Apparently, in a picture with propagators for the bare states, series of excitations enclosing each other without crossing are generated. The ENCA-scheme introduces the vertex corrections up to second order in the hybridization and thus incorporates many more processes with crossing band-electron lines. For the Anderson model it was shown to improve considerably on the SNCA, reproducing e.g. the correct Kondo scale [16].

In the generalization to our multi-orbital model the ENCACF incorporates vertices like the one shown in Fig. 1(b).

This example suffices to clarify the building principle of the approximation. The other two vertex functions appearing in Fig. 1(a) are constructed in an analogous fashion. They depend on two energy variables, one of them complex, and have to be treated in all analytical equations with great care; numerically, their inclusion considerably enlarges the calculational effort. We will not make explicit all the diagrammatic self-energy equations needed and the corresponding additional set of diagrams necessary to build up the one-particle-Green function consistently in ENCACF. In principle, the diagrams are ob-

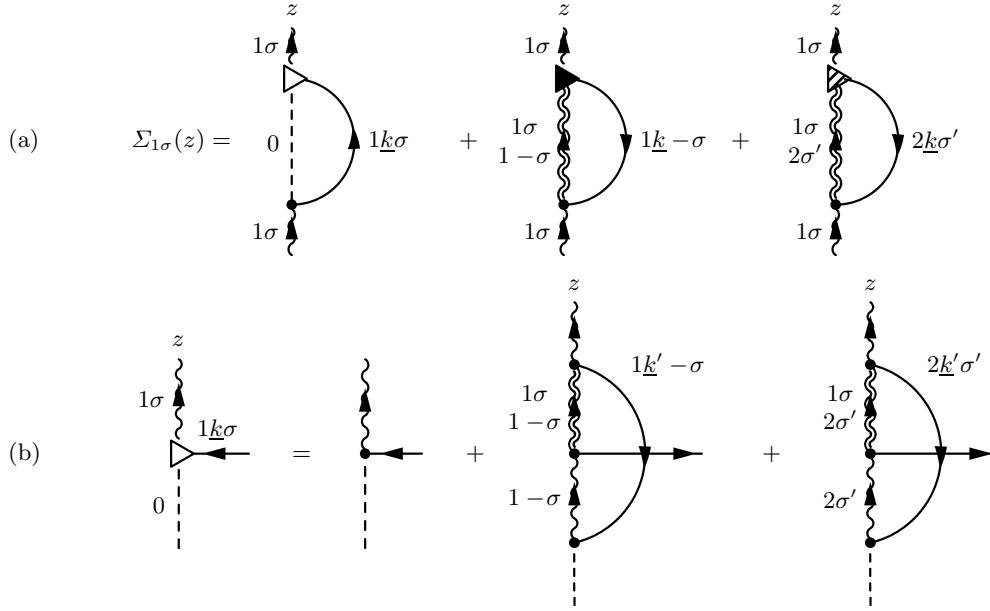


**Fig. 1.** Diagrammatic representation of ionic self-energies (a) and vertex corrections (b) for a single-impurity Anderson model (SIAM) in direct perturbation theory. Physical processes are arranged vertically along an imaginary time axis (broken line) which bears an energy variable  $z$  after Laplace-transformation. Presence of an electron in the local shell is indicated via a wiggly line on this time axis. Excitations of band electrons (straight lines) take place at hybridization vertices (dots on the time axis). All line crossings in these diagrams can be attributed as a correction to one of the vertices, which are drawn as triangles.

tained from the ones of Fig. 1 and the additional ones not shown, by cutting one band electron line. Following the remarks above and the well known recipes for a transcription of such diagrams into formulas [32,12] it is a straightforward task to complete the systems of integral equations for local propagators and for defect propagators [35], as well as to assemble all contributions to the Green functions and the excitation spectra derived from them.

We have solved the full ENCACF equations to convergence and will present one-particle excitation spectra derived from Green functions according to

$$\rho_{jl\sigma}(\omega) = -\frac{1}{\pi} \text{Im} \langle \langle \hat{f}_{j\sigma} | \hat{f}_{l\sigma}^\dagger \rangle \rangle (\hbar\omega + i\delta) \quad (j, l = 1, 2) \quad . \quad (2)$$

In most cases we will present the complete spectrum

$$\rho_\sigma(\omega) = \sum_j \rho_{jj\sigma}(\omega) \quad , \quad (3)$$

which in our case is normalized to 2, since it contains excitations of both local levels  $\epsilon_1$  and  $\epsilon_2$  with definite spin  $\sigma$ . First we compare a typical calculation with some simpler cases, which in part are known from the literature.

In Fig. 2 we present the a ENCACF-spectrum, a SNCACF to identify the bare values of transition energies. These are for  $U = 2$ :  $\Delta\epsilon_1^{(0)} = E_{1;1} - E_0 = \epsilon_1 = -1$ ,  $\Delta\epsilon_2^{(0)} = E_{1;2} - E_0 = \epsilon_2 = -0.5$ ,  $\Delta\epsilon_3^{(0)} = E_{2;11} - E_{1;1} = \epsilon_1 + U = 1$ ,  $\Delta\epsilon_4^{(0)} = E_{2;12} - E_{1;1} = \epsilon_2 + U = 1.5$ ,  $\Delta\epsilon_5^{(0)} = E_{2;12} - E_{1;2} = \epsilon_1 + U = 1$  and  $\Delta\epsilon_6^{(0)} = E_{2;22} - E_{1;2} = \epsilon_2 + U = 1.5$ . Apparently in a region of energies  $\omega$  between +1 and +2 considerable spectral weight is accumulated. The resonances acquire widths on the one-particle scale  $\Delta$  and in excess thereof via the local interactions and can therefore in part

SNCACF with the same value of  $U = 2$  reveals this still to be true in the multi-orbital model: In fact, the spectral weight accumulated near the chemical potential at  $\omega = 0$  is much larger in the first case, although the two different temperatures likewise approximately reflect the respective approximations to the Kondo scales of the model without the second orbital (see inset of Fig. 2).

A comparison with the SNCACF-spectrum at larger  $U = 4$  demonstrates the shortcomings of a simplified calculation, where all doubly occupied states are projected out via letting  $U$  go to infinity: Considerable spectral weight is driven out of the band region, in form of increasingly narrow spikes. The ENCA-calculation without the second orbital, finally, helps to identify the additional spectral weight induced by the level  $\epsilon_2$ , not only in the region of high excited states around  $\omega \approx 2$ , but also near  $\omega = 0$ , where the many-body resonance acquires two satellites above and below. In a qualitative sense this behavior is known from earlier calculations using SNCA and  $U = \infty$  [36,37]. Although the number of one-particle transitions contributing to these spectra is rather small due to the uniform value of Coulomb-matrix elements and to the restriction to the subspace with  $n_{loc} \leq 2$ , is it worthwhile

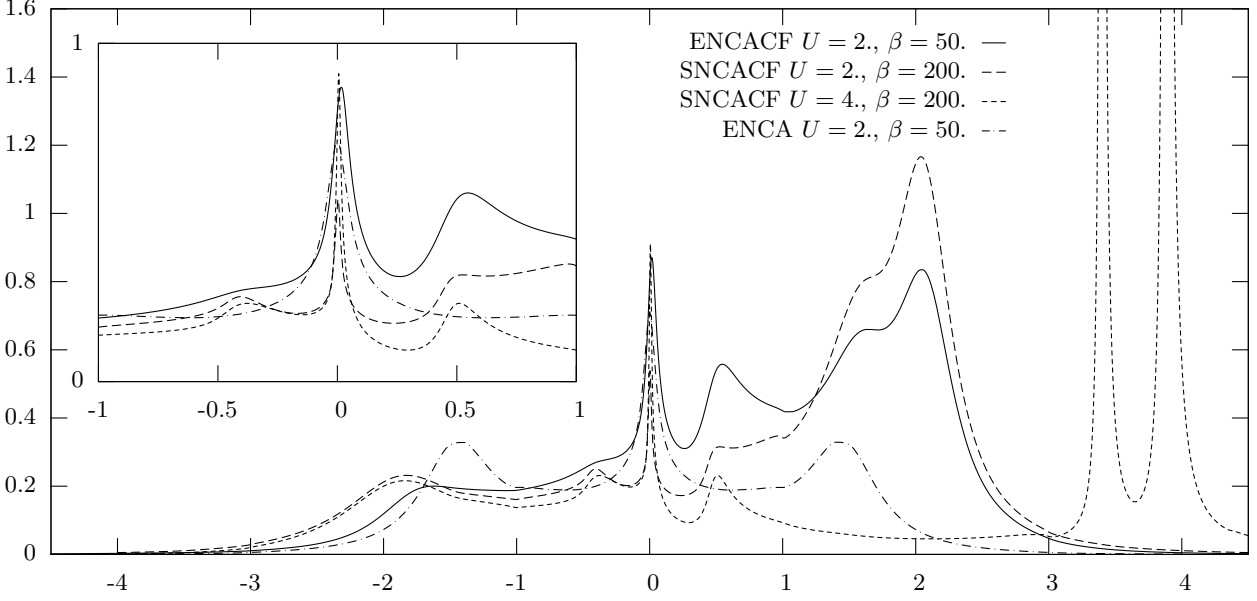


**Fig. 2.** Local one-particle excitation spectrum of the two-orbital model (first three curves) and of a corresponding Anderson model with one orbital, calculated within SNCACF and ENCACF, respectively. The temperature  $T = \frac{1}{\beta k_B} = \frac{1}{200 k_B}$  for the two SNCACF calculations is chosen higher than in the two ENCACF cases, so that it becomes comparable with the approximate Kondo scale in each case. Other model parameters are  $\epsilon_1 = -1$ ,  $\epsilon_2 = 0.5$ ,  $\Delta = \pi \rho^{(0)}(0) = 0.3$  (Anderson width) and  $U_{11} = U_{22} = U_{12} = 3$ ; energies are in units of the  $3d=6^{th}$  part of the width of a simple cubic bandstructure.

not be well resolved individually. The resonance originating from  $\Delta\epsilon_1^{(0)}$ , i.e. the lowest peak in the figure is known to be broadened by  $2 \cdot \Delta$  in a pure ENCA-calculation without the higher local level due to the blocking of the resonance, if an electron with opposite spin already resides there [36]. This blocking effect apparently is enhanced by the presence of the second local level.

The visibility of excitation peaks in these spectra is largely determined by the thermal occupation probability of the initial and final shell state. Whereas e.g. the transition  $\Delta\epsilon_1^{(0)}$  possesses a weight  $\langle \hat{P}_0 \rangle + \langle \hat{P}_{1;1\sigma} \rangle \approx \frac{1}{2}$  ( $\langle \hat{P}_M \rangle$  being the thermal occupation number of the local shell-state  $M$  with  $\hat{P}_M$  the corresponding projection operator), the next transition at  $\Delta\epsilon_2^{(0)}$  has negligible weight  $\langle \hat{P}_0 \rangle + \langle \hat{P}_{1;2\sigma} \rangle \ll 1$  in the regime considered here, with single local occupation in level  $\epsilon_1$  being by far most probable. The high-lying peaks in the  $U = 4$ -case shown in 2, likewise have weight near 1, but already indicate a crossover to narrow spikes, since broadening begins to decrease due to a lack of nearby band states. In this way, the rough features of single particle excitation spectra can completely be classified.

### 3 Discussion of one-particle excitation spectra and correlation effects

Figs. 3 and 4 are designed in order to identify correlation effects in the spectra, and in particular the influence of the presence of the second local one-particle level with

higher energy  $\epsilon_2 > \epsilon_1$ . A clear hint to the important role of many-body correlations, beyond the interaction-induced splitting of the local levels into a lower part at about  $\epsilon_j$  and a higher part near  $\epsilon_j + U$  both with fractional weights, is a pronounced temperature dependence in a certain interval of energies  $\omega$ .

Fig. 3 shows sequences of spectra for varying temperature, typically reaching from about a third of a characteristic low energy scale  $k_B T^*$  ( $\beta = 100$ ) up to about ten times  $k_B T^*$ . A value of about  $k_B T^* \approx \frac{1}{30}$  can be deduced from the half-width of the narrow peak at  $\omega = 0$ ; it would coincide with the Kondo scale  $k_B T_K$ , if the higher local level were not involved. Nevertheless, the choice of parameters for the figures implies a situation like the one found in the classical Kondo regime, with  $\epsilon_2 = -0.8$  or  $-0.5$  clearly larger than  $\epsilon_1 = -1$ , both negative, but  $U_{11} = U_{22} = U_{12}$  large enough to favour a ground state occupation  $n_{loc} = \sum_{j=1,2} \sum_{\sigma} n_{j\sigma} \approx 1$ . In both cases of Fig. 3, for  $\epsilon_2 - \epsilon_1 = 0.2$  small (part a) and for  $\epsilon_2 - \epsilon_1 = 0.5$  larger (part b), the curves in a narrow region around the chemical potential  $\omega = \mu = 0$  prove to be strongly temperature dependent, whereas the remote parts of the spectra are much less affected by temperature variations. The qualitative picture, known from earlier work, of a three peak many-body resonance forming when  $T^*$  is approached from above is clearly seen in Fig. 3(b). In Fig. 3(a), however, the lowest and weakest of these peaks is concealed as a very flat shoulder on the left side of the main resonance in the middle. This result again demonstrates the stronger lifetime effects seen in the ENCACF as compared to a simpler SNCACF-calculation, which tend to broaden the

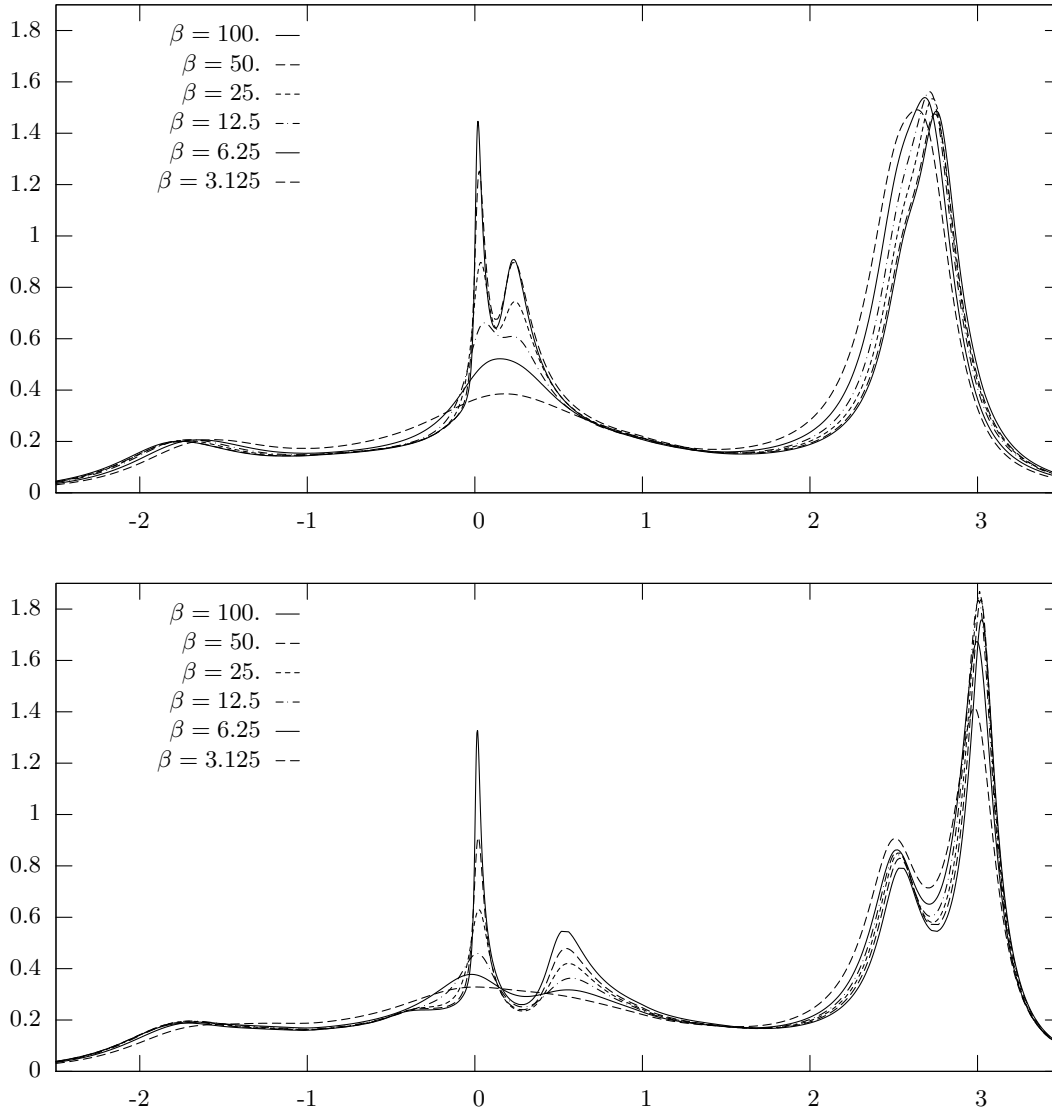


**Fig. 3.** Temperature dependence of the local one-particle excitation spectrum of the two-orbital model in ENCACF-approximation. Parts (a) and (b) differ in the value of the second local particle level  $\epsilon_2 = -0.8$  and  $\epsilon_2 = -0.5$ , respectively. Other model parameters are as in Fig. 2.

resonances further and increase the scale  $T_K$  considerably. The origin of the three-peak structure has been explained consistently [36]: The ASR of the Kondo scenario acquires two satellites, one on each side, due to additional local excitations in the spectral region shaped by the many body effects. A local excitation from level  $\epsilon_1$  to level  $\epsilon_2$  preserves the possibility of forming a Kondo singlet of different kind, and the corresponding new ASR is shifted via the foregoing excitation process by  $\Delta\epsilon = \epsilon_2 - \epsilon_1$  above the chemical potential. The inverse process leaves its trace near  $\omega = -\Delta\epsilon$ ; its thermal weight however, is reduced by the small occupation probability  $\epsilon_2$  compared to the lower level  $\epsilon_1$ .

Fig. 4 demonstrates more clearly that this interpretation in fact holds true: The two side peaks of the main resonance actually move with the position of the higher

local level  $\epsilon_2$  and correspondingly also become less pronounced with growing distance. The higher energy satellite can nevertheless be followed through the high energy region around and above  $\epsilon_1 + U = 2$ ; it appears in the curve for  $\epsilon_2 = 2$  on the right hand side of this peak, but below the peak at energy  $\epsilon_2 + U = 5$ . The choice of parameters for this case according to the listing of excitation energies in the last section, only give unperturbed peak positions at  $\Delta\epsilon_1^{(0)} = \epsilon_1 = -1$ ,  $\Delta\epsilon_2^{(0)} = \Delta\epsilon_3^{(0)} = \Delta\epsilon_5^{(0)} = \epsilon_2 = \epsilon_1 + U = 2$ ,  $\Delta\epsilon_4^{(0)} = \Delta\epsilon_6^{(0)} = \epsilon_2 = \epsilon_2 + U = 5$ , so that the given identification of the feature near  $\omega = 3.3$  seems to be unique. The temperature chosen via  $\beta = 50$ , for Fig. 3 and all the following ones corresponds to  $T^*$  or somewhat lower, so that all many-body effects should clearly be visible.

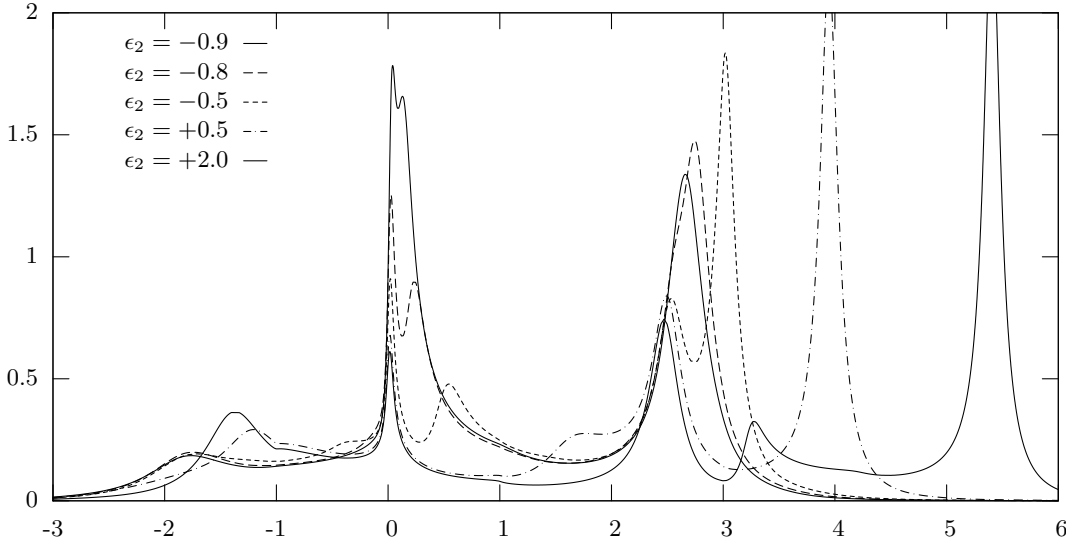


**Fig. 4.** Dependence of the local one-particle excitation spectrum of the two-orbital model on the position of the second level  $\epsilon_2$  in ENCACF-approximation. The temperature  $\frac{1}{50k_B}$  compares roughly with the Kondo scale, other model parameters are as in Fig. 2.

Also the energy region below the chemical potentials reveals some interesting features. In particular, the way in which the exact form of the lower main resonance of the original Anderson model without the higher local level is reconstructed with growing  $\epsilon_2$ , allows to identify the amount of additional scattering due to the blocking between electrons in levels  $\epsilon_1$  and  $\epsilon_2$ . Even here, the lower and weaker side peak can be traced for a limited region of increasing  $\epsilon_2$ -values as a shallow flank, although its thermal weight decreases and it is obscured somewhat by the changing form and position of the main resonance arising from  $\Delta\epsilon_1^{(0)} = \epsilon_1 = -1$ . The increase of the center of this broad main resonance with growing  $\epsilon_2$  reflects the loss in ground state energy, when level interactions become weaker. The shrinking width of this resonance indicates the loss of blocking of level  $\epsilon_1$  due to the presence of electrons in level  $\epsilon_2$ , when this energy increases.

The next figures are devoted to a study of the influence, which the magnitude of local Coulomb-matrix elements has on the spectra and on the correlations. In Fig. 5 we keep the equality  $U_{11} = U_{22} = U_{12} \equiv U$ , but vary  $U$  in integer steps from 2 to 5. Unlike the variation of temperature in Fig. 3 or the variation of the upper level position in Fig. 4 the variation of  $U$  does affect the width of the central many-body resonance. This  $T^*$  gets smaller with increasing  $U$  in accord with the behavior of  $T_K$  in the Kondo effect. The decrease of  $T^*$  is moderate and effectively stops when the upper resonances  $\epsilon_1 + U$  and  $\epsilon_2 + U$  cross the upper band edge at  $\omega = 3$ . The splitting of these two highest peaks is fixed approximately at our value of  $\epsilon_2 - \epsilon_1 = 0.5$ , with  $\epsilon_1 = -1$ . The width of both peaks decreases from  $U = 3$ , in which case they just stay inside the band region, to  $U = 5$ , where both are situated above it. Increased scattering inside the region with high density of band states washes these peaks out which best can be

seen in the region  $1 < \omega < 2.5$  for the lowest value  $U = 2$ . The height of the central many-body resonance changes only slightly, showing that we stay in the near saturated region  $T \lesssim T^*(U)$ .

A very interesting perspective opens when variations of the Coulomb matrix element  $U_{12}$ , i.e. the repulsion between electrons in different local levels  $\epsilon_1$  and  $\epsilon_2$ , are performed keeping  $U_{11} = U_{22}$  fixed. Fig. 6 shows the corresponding spectra, again for fixed  $\epsilon_1 = -1$ ,  $\epsilon_2 = -0.5$ ,  $\beta = 50$  and  $U_{11} = U_{22} = 3$ , and for a variation of  $U_{12}$  in integer steps between 0 and 5. It is apparent, that a considerable transfer of spectral weight from above to below the chemical potential takes place when going from values  $U_{12} \geq 1$  to values  $U_{12} \approx 0$ . In fact, the condition  $\epsilon_2 + U_{12} = 0$ , i.e.  $U_{12} = 0.5$  marks a crossover here: For  $U_{12} > 0.5$  a ground state with single level occupation  $n_{loc} = 1$  is stable in zeroth order as in all cases before, whereas for  $U_{12} < 0.5$  the stability goes over to a new ground state with  $n_{1\sigma} = n_{2\sigma} = \frac{1}{2}$ , i.e.  $n_{loc} = \sum_{j\sigma} n_{j\sigma} = 2$ . This changes drastically the thermal occupation probabilities of local shell states and the corresponding transitions as well as the nature of the many-body correlations.

Generally, the thermal weight of a one-particle transition from shell state  $M$  to  $M'$  is  $\langle \hat{P}_M \rangle + \langle \hat{P}_{M'} \rangle$ , i.e. the sum of the occupation probabilities if the initial and the final state, in zeroth order. The corresponding excitation energy is  $\Delta\epsilon = E_{M'} - E_M$  and  $n_{loc} = n_{loc} + 1$  by definition. For large  $U_{12}$  and  $\epsilon_1 < \epsilon_2$  in the regime considered here,  $\langle \hat{P}_{1;1\sigma} \rangle$  is approximately  $\frac{1}{2}$  and all other  $\langle \hat{P}_M \rangle$  are small. Consequently, the transitions with energies  $\Delta\epsilon_1^{(0)} = E_{1;1} - E_0 = \epsilon_1$ ,  $\Delta\epsilon_3^{(0)} = E_{2;11} - E_{1;1} = \epsilon_1 + U_{11}$  and  $\Delta\epsilon_4^{(0)} = E_{2;12} - E_{1;1} = \epsilon_2 + U_{12}$  are strongly and the others are weakly represented in the spectra. For i.e.  $U_{12} = 4$  this explains the 3-peak structure in the high

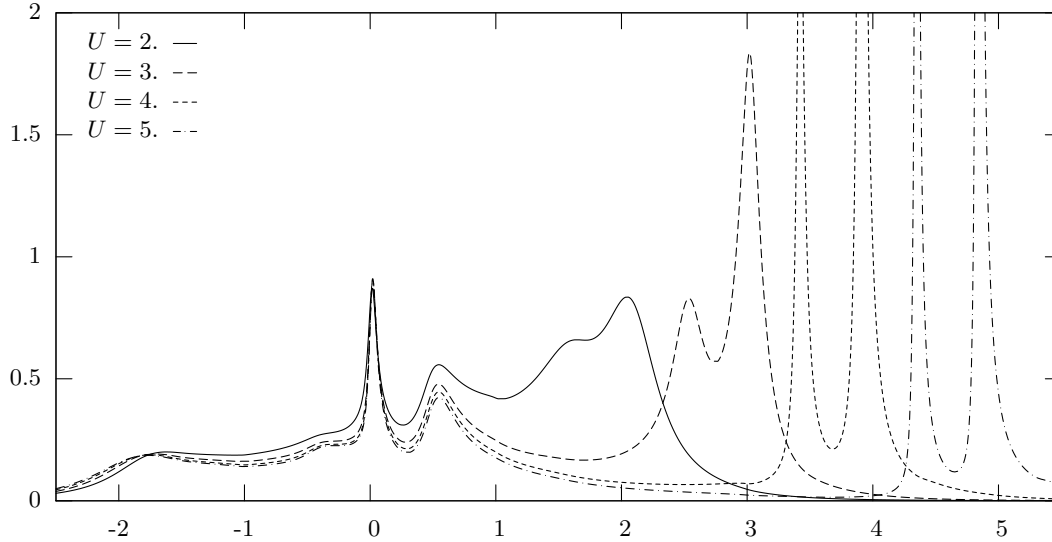


**Fig. 5.** Dependence of the local one-particle excitation spectrum of the two-orbital model on the Coulomb matrix element  $U$  for the case  $U_{11} = U_{22} = U_{12}$  in ENCACF-approximation. The temperature and second level position are  $\frac{1}{50k_B}$  and  $\epsilon_2 = -0.5$ , respectively. Other model parameters are as in Fig. 2.

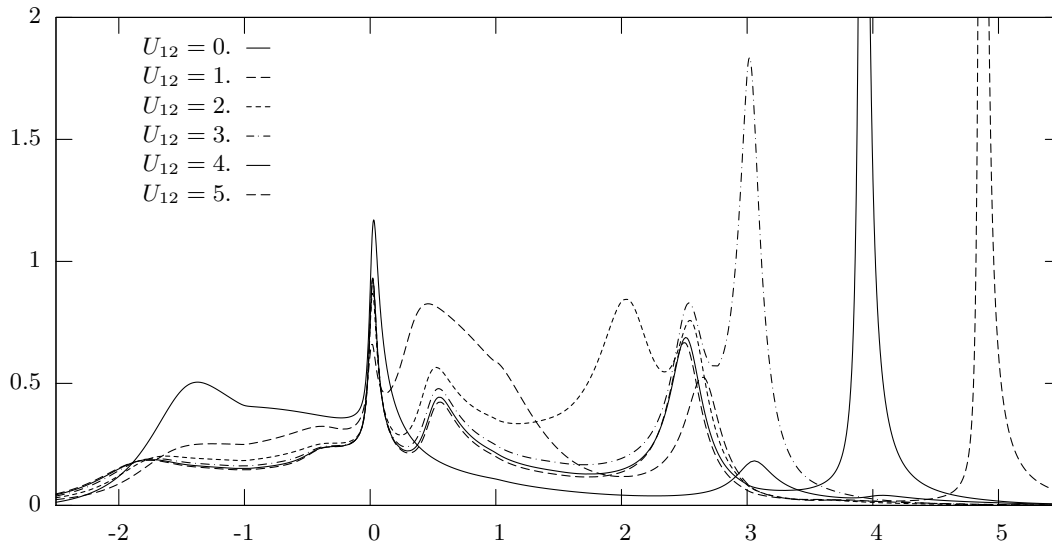


**Fig. 6.** Dependence of the local one-particle excitation spectrum of the two-orbital model on the particular size of  $U_{12}$  of the Coulomb-repulsion between an electron in level  $\epsilon_1$  and one in level  $\epsilon_2$  in ENCACF-approximation. Other model parameters are as in Fig. 2.

energy region with peaks shifted somewhat outward from  $\Delta\epsilon_1^{(0)} = -1$ ,  $\Delta\epsilon_3^{(0)} = 2$ , and  $\Delta\epsilon_4^{(0)} = 3.5$ . For small  $U_{12}$ , on the other hand,  $\langle \hat{P}_{2;1\sigma 2\sigma'} \rangle$  is approximately  $\frac{1}{4}$  and the other probabilities are small, so that only the transitions with energy  $\Delta\epsilon_4^{(0)}$  and  $\Delta\epsilon_5^{(0)} = E_{2;12} - E_{1;2}$  are strong and the others weak. The values i.e. for  $U_{12} = 0.5$  are  $\Delta\epsilon_4^{(0)} = 0$  and  $\Delta\epsilon_5^{(0)} = -0.5$ , for  $U_{12} = 0$  one obtains  $\Delta\epsilon_4^{(0)} = -0.5$  and  $\Delta\epsilon_5^{(0)} = -1$ .

These considerations already give a rough explanation for the observed shift of spectral weight, if one takes into

account that peak positions are usually renormalized away from the chemical potential by interactions. The crossover region itself bears interesting physics in it. At the point  $U_{12} = 0.5$ ,  $\epsilon_1 = -1$  and  $\epsilon_2 = -0.5$  as before, the two states  $E_{1;1} = \epsilon_1 = -1$  and  $E_{2;12} = \epsilon_1 + \epsilon_2 + U_{12} = -1$  with single and double occupancy are degenerate ground states in zeroth order, which puts the system in some kind of intermediate valence regime. This corresponds well with a broad distribution of spectral weight near  $\omega = 0$ . The effect is seen in the curve for  $U_{12} = 1$ , and even more pronounced, in the following Fig. 7 for  $U_{12} = 1$ , with  $\epsilon_1 = \epsilon_2 = -1$ .

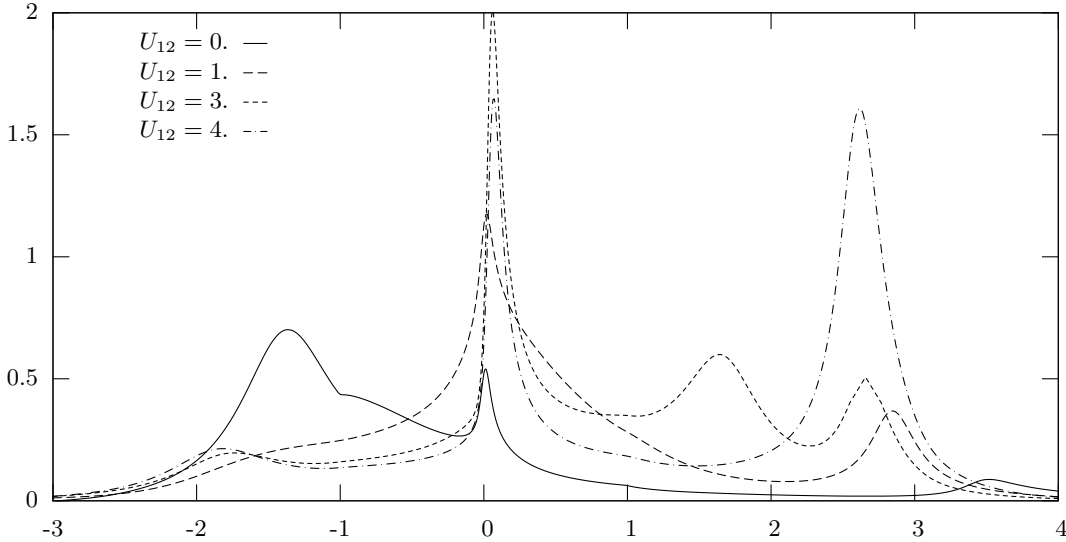


**Fig. 7.** Like Fig. 6, but for  $\epsilon_1 = \epsilon_2 = -1$ , i.e. the two local levels  $\epsilon_1$  and  $\epsilon_2$  are equally occupied and contribute symmetrically, i.e. to separate Kondo effects at  $U_{12} = 0$ .

Consistently, in Fig. 7, for vanishing  $U_{12} = 0$  a marked Kondo effect with a thin ASR near  $\omega = 0$  reappears. In this case the ground state  $E_{2;12} = -2$  is well separated from the first excited states  $E_{1;1} = E_{2;2} = \epsilon_1 = -1$ .

With respect to the local many-body correlations the crossover scenario implies the following consequences:  $U_{12}$  can be viewed as a measure for the competition between tendencies to occupy each of the two local levels. For large  $U_{12} > U_{11}$  this competition favors the lower local level  $\epsilon_1$  and its corresponding Kondo effect. Level  $\epsilon_2$  then is only populated with a small probability and furnishes only small side peaks near the ASR. Correlations due to a virtual Kondo effect of level  $\epsilon_2$  stay incomplete. With  $U_{12} \approx U_{11} = U_{22}$  reaching the value of the other Coulomb-matrix elements all of the different forms of local double occupancy become energetically comparable, so that the side peaks are strengthened somewhat due to increased interference of the correlations. Below the crossover to the doubly occupied ground state, however, individual Kondo effects for level  $\epsilon_1$  and  $\epsilon_2$  start to emerge. They do not show up for small absolute values of  $\epsilon_1$  and  $\epsilon_2$ , where ground states with different local occupancy have comparable energies (on the scale of the Anderson width) and low-lying charge fluctuations cause a broad peak near  $\omega = 0$ . If  $\epsilon_1$  and  $\epsilon_2$  are both well below the chemical potential a complete decoupling then occurs at the point  $U_{12} = 0$ , where each of the levels only interacts with its own band of the same symmetry. Due to different level positions the two Kondo temperatures  $T_{Kj} \sim \exp(-\frac{1}{J_j \rho_\sigma^{(0)}(0)})$ ,  $J_j \approx \frac{V^2}{|\epsilon_j|} + \frac{V^2}{\epsilon_j + U_{jj}}$  may come out largely different, as a possibility. With e.g.  $T_{K1} < T < T_{K2}$  the ASR due to  $\epsilon_2$  is completely formed, whereas the one due to  $\epsilon_1$  is still in an early stage; the low-energy excitations then would be largely determined by the Kondo effect of the higher lying local level.

For our set of parameters  $T_{K2}$  should be considerably higher than  $T_{K1}$ , and the position of  $\epsilon_2 = -0.5$  indicates an intermediate valence region. The corresponding ‘‘ASR’’ then significantly broadens and acquires some degree of linewidth via charge fluctuations and simple one-particle scattering  $\propto V^2$ . Thus due to the role of temperature variations relative to  $T_{K1}$  and  $T_{K2}$  and due to different level positions  $\epsilon_2$  in the interval between  $\epsilon_1$  and the chemical potential  $\mu = 0$ , the crossover scenario presented here can involve quite different shapes of the one-particle excitation spectrum. In particular, when even more complicated multi-orbital models are used e.g. in calculations of correlated bandstructures, great care seems necessary to understand and control all parts of the calculation and the physical relevance of all features. We will elaborate on this cautionary remark below also in connection with some technical aspects of the approximations used.

With Fig. 8 we present further evidence to support our picture of the crossover scenario. We have resolved spectra from Fig. 6 on each site of the crossover, into the partial spectra, which incorporate only the excitation on one of the local levels. Fig. 8 clearly demonstrates the strong dominance of the Kondo effect on the lower level  $\epsilon_1$  when  $U_{12}$  is large: The ASR seen for  $U_{12} = 4$  is completely contained in the partial spectrum  $\rho_{1\sigma}(\omega)$ , whereas  $\rho_{2\sigma}(\omega)$  is continuously flat near  $\omega = 0$ , although  $T = \frac{1}{50k_B}$  is of the order of a hypothetical  $T_{K2}$  of an isolated level  $\epsilon_2$ . In Fig. 7 on the other hand, we have seen a symmetrical situation with  $\epsilon_1 = \epsilon_2 = -1$ . The ASR, which shows up for  $U_{12} = 0$ , is clearly shared in equal parts by both partial spectra. A similar effect in the spectrum with lowest  $U_{12}$  of Fig. 6 is not seen due to the different nature of correlations in the Intermediate Valence regime.

The regime with the doubly occupied local ground state is apparently not as well described by our ENCACF-approximation (not to mention the simpler SNCACF) as

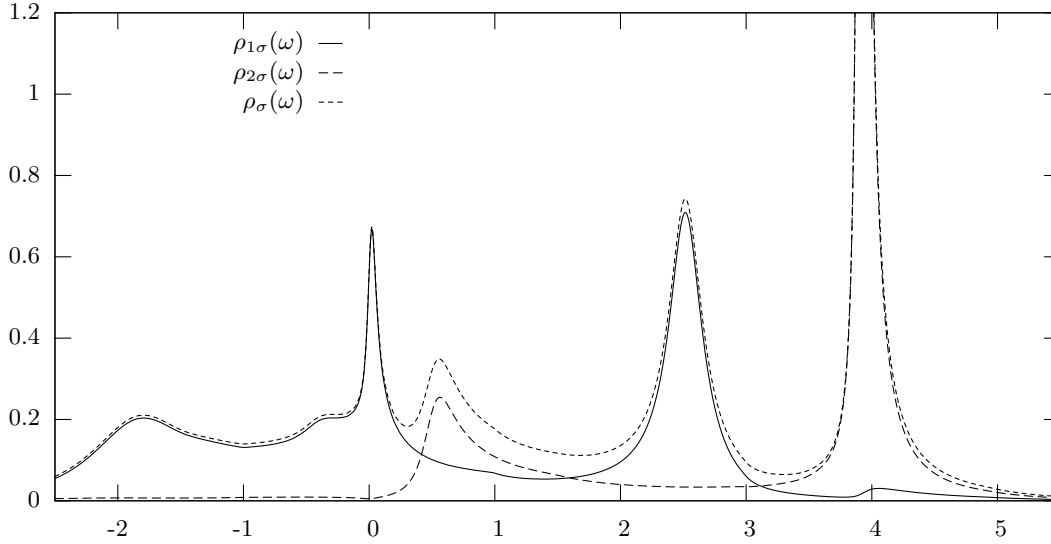


**Fig. 8.** Partial local one-particle excitation spectra  $\rho_{1\sigma}(\omega)$ ,  $\rho_{2\sigma}(\omega)$  in comparison with the combined spectrum  $\rho_\sigma(\omega) = \rho_{1\sigma}(\omega) + \rho_{2\sigma}(\omega)$ . The model parameters are as in Fig. 6 with  $U_{12} = 4$ .

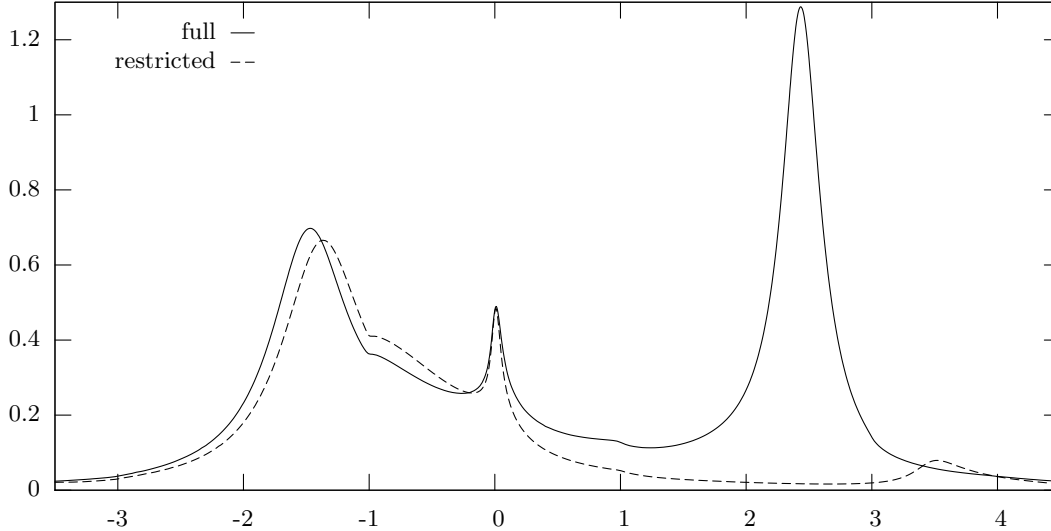


**Fig. 9.** Local one-particle excitation with restricted (local occupancy  $\leq 2$ ) and full (local occupancy  $\leq 4$ ). The model parameters are as in Fig. 7 with  $U_{12} = 0$ .

the former regime with the singly occupied local ground state. A plain hint comes from the lack of spectral intensity in the high energy region above  $\omega = 0$ . More subtle is a corresponding influence on the correlations determining the spectrum nearby the chemical potential. With a local ground state derived from  $E_{2;12} = \epsilon_1 + \epsilon_2 + U_{12}$  and  $U_{12}$  small, excitations to a local state with triple occupancy and energy  $\epsilon_1 + 2\epsilon_2 + U_{12} + U_{22}$ , i.e.  $\Delta\epsilon_7^{(0)} = \epsilon_2 + U_{22}$ , or energy  $2\epsilon_1 + \epsilon_2 + U_{12} + U_{11}$ , i.e.  $\Delta\epsilon_8^{(0)} = \epsilon_1 + U_{11}$ , contribute to the dynamics. Their importance compares with that of  $\Delta\epsilon_4^{(0)} = \epsilon_2 + U_{12}$  and  $\Delta\epsilon_5^{(0)} = \epsilon_1 + U_{12}$ , similar to the importance of both one-particle excitations at  $\epsilon_1$  and  $\epsilon_1 + U$  for an Anderson model with finite  $U$ . This deficiency can

only be cured, when the Hilbert space underlying the calculations is enlarged to account for triple ( and quadruple) local occupancy. Thereby the system of integral equations for propagators again becomes considerably enlarged.

We have also solved the correspondingly completed ENCACF-theory numerically and present a spectrum in Fig. 9. It is calculated for the most interesting case of  $\epsilon_1 = \epsilon_2 = -1$ ,  $U_{12} = 0$  and  $U_{11} = U_{22} = 3$ ,  $\beta = 50$  and is compared with the incomplete spectrum discussed before. The difference, particularly in the high-energy region is clearly visible. On the other hand these differences for cases, where the local ground state is singly occupied, es-

sentially only show up at very high excitations energies  $\omega > 2U$  and can safely be ignored.

A second technical remark also refers to our note of caution made above. Although from a puristic point of view and in agreement with physical insight, the system for  $U_{12} = 0$  decouples dynamically into two independent ones, this is in general not realized in approximate version of direct perturbation theory, which from the beginning incorporates  $U_{12}$  into the unperturbed local system. For example, with  $U_{12} = 0$  and  $\epsilon_j < -\Delta_j < 0 < \Delta_j < \epsilon_j + U_{jj}$  ( $j = 1, 2$ ), one should observe two independent Kondo effects. Although as we have demonstrated, this is actually found for large enough absolute values of both  $\epsilon_j$ , we are not so confident about our findings in the crossover regime. The point can be visualized with Fig. 1(a). The third self-energy diagram shown there has an intermediate state  $n_1 = n_2 = 1$ , which is the ground state for small  $U_{12}$ . Fluctuations like the one shown via the downrunning band electron line, as projected on the dynamics of level  $\epsilon_1$ , can only take place when an electron is present in level  $\epsilon_2$ . This establishes a spurious kind of correlation, which only is eliminated from the calculation when all of the possible vertex corrections are actually taken into account in the vertex shown at the top. Only this can lead to all combinations of individual time orders, which together would decouple the two subsystems.

Our ENCACF captures the leading part thereof via the vertex corrections shown in figure 1(b). It is, however, not settled yet how important higher contributions with more crossings are in the different regimes. Although there is some experience for the simple Anderson model [38, 37, 18], suggesting a qualitatively well behaved ENCA, in particular the crossover regime found here might need even better approximations.

## 4 Conclusion and Perspective

Our investigation of a multi-orbital model with a new crossing approximation, the ENCACF, which goes beyond a simple modification of NCA and works for all finite values of Coulomb parameters, has revealed a variety of possible forms of one particle excitation spectra. We have studied the role of different model parameters, temperature  $T$ , energies  $\epsilon_j$  of the two local one-particle levels with different symmetry, and of the Coulomb-matrix elements  $U_{jl}$  between electrons in level  $\epsilon_j$  and  $\epsilon_l$ . Different regimes could be characterized, according to the nature of the local ground state and of the local correlations. These regimes exhibit different modified forms of a Kondo effect, when the levels  $\epsilon_1$  and  $\epsilon_2$  are below the chemical potential and representative values of  $U_{jl}$  are large enough.

Single particle transition between local states on the one hand and traces of many-body correlations on the other hand could both be identified in the calculated spectra and were discussed in a consistent framework. The crossover between regimes of different local groundstate occupancy involves interesting Intermediate Valence phenomena, where charge fluctuations intervene. We have pointed to the intricate physics, which determines the crossover

region, and to some problems of approximations which possibly render a complete understanding difficult with the methods developed so far. Particular caution seems necessary when interpreting e.g. experimental data from photoelectron spectroscopy with insufficient approximations, using e.g. simpler forms of direct perturbation theory like NCA, combined with the limit of infinite local Coulomb repulsion. Whereas we believe, that some correct qualitative information can be gathered in this way and a correct overall picture be developed, our new calculations show, based on an essentially improved theory, show that quantitative fits may be very misleading: The relevant many-body scale, for example grossly differs and important spectral information from the high energy region gets lost. Moreover, even the detailed spectral intensities in the low energy region depend on the rest of the spectrum and may come out incorrectly, in particular in real physical parameter regimes of transition metal ions which do not allow for an argument of universality. Nevertheless, our results also support some earlier findings, in particular for the spectroscopy of metallic compounds with Ce-atoms. For the use of multi-orbital models of the kind studied in connection with self-consistent methods for correlated band structures, on the other hand, our investigation furnishes a rather poor perspective due to the complexity of the problem and the insufficient quality of suitable impurity solvers proposed so far. Here we hope that generalizations of our ENCACF may be helpful.

In any case, multi-orbital impurity solvers for lattice systems with strong local correlations in most cases should be planned in an even more general form than our model of equation (1). The reason simply is that symmetry decompositions of band states around different sites as centers are not compatible: They combine the Bloch functions in a different way. As a consequence, the medium around a given representative site will mix the symmetry-decompositions, i.e.  $\epsilon_{1\mathbf{k}}$  and  $\epsilon_{2\mathbf{k}}$  in our model. In that case the possible diagrammatic processes make up a larger set as before, with the consequence that the irreducible self-energies of ionic propagators become a matrix. This matrix involves also elements which are non-diagonal in the level indices  $j$ . The same complication arises in e.g. the case, where an impurity complex made up of two sites is inserted into a perfect crystal with orbitals on each of the two sites. This again spoils the conservation of a  $j$  quantum number of local electrons and leads to the same consequences as before. We have taken up studies of such generalized multi-orbital models and will report on results in a forthcoming paper.

## References

1. G. Grüner, A. Zawadowski, Rep. Prog. Phys. **37**, 1497 (1974)
2. H.R. Krishna-murthy, J.W. Wilkins, K.G. Wilson, Phys. Rev. B **21**(3), 1003 (1980)
3. H.R. Krishna-murthy, J.W. Wilkins, K.G. Wilson, Phys. Rev. B **21**(3), 1044 (1980)

4. T. Pruschke, M. Jarrell, J. Freericks, *Adv. Phys.* **44**, 187 (1995)
5. A. Georges, G. Kotliar, W. Krauth, M.J. Rozenberg, *Rev. Mod. Phys.* **68**(1), 13 (1996)
6. C. Grenzbach, F.B. Anders, G. Czycholl, T. Pruschke, *Phys. Rev. B* **74**(19), 195119 (17) (2006), <http://link.aps.org/abstract/PRB/v74/e195119>
7. J.E. Hirsch, R.M. Fye, *Phys. Rev. Lett.* **56**(23), 2521 (1986)
8. P. Werner, A. Comanac, L. de' Medici, M. Troyer, A.J. Millis, *Phys. Rev. Lett.* **97**(7), 076405 (4) (2006), <http://link.aps.org/abstract/PRL/v97/e076405>
9. K.G. Wilson, *Rev. Mod. Phys.* **47**(4), 773 (1975)
10. R. Peters, T. Pruschke, F.B. Anders, *Phys. Rev. B* **74**(24), 245114 (12) (2006), <http://link.aps.org/abstract/PRB/v74/e245114>
11. H. Keiter, J.C. Kimball, *J. Appl. Phys.* **42**(4), 1460 (1971)
12. H. Keiter, G. Morandi, *Phys. Rep.* **109**(5), 227 (1984)
13. N. Grewe, *Z. Phys. B* **53**(4), 271 (1983)
14. H. Kojima, Y. Kuramoto, M. Tachiki, *Z. Phys. B* **54**(4), 293 (1984)
15. N.E. Bickers, *Rev. Mod. Phys.* **59**(4), 845 (1987)
16. T. Pruschke, N. Grewe, *Z. Phys. B* **74**, 439 (1989)
17. K. Haule, S. Kirchner, J. Kroha, P. Wölfle, *Phys. Rev. B* **64**(15), 155111 (2001)
18. N. Grewe, S. Schmitt, T. Jabben, F.B. Anders, *J. Phys.: Condens. Matter* **20**, 365217 (2008)
19. N. Grewe, *Z. Phys. B* **52**(3), 193 (1983)
20. Y. Kuramoto, *Z. Phys. B* **53**, 37 (1983)
21. K. Held, I.A. Nekrasov, G. Keller, V. Eyert, N. Blmer, A.K. McMahan, R.T. Scalettar, T. Pruschke, V.I. Anisimov, D. Vollhard, *Phys. Status Solidi B* **243**(11), 2599 (2006)
22. N. Grewe, *Ann. Phys. (Leipzig)* **14**(9-10), 611 (2005)
23. K. Held, O.K. Andersen, M.F. and A. Yamasaki, Y.F. Yang, *J. Phys.: Condens. Matter* **20**, 064202 (2008)
24. M. Garnier, K. Breuer, D. Purdie, M. Hengsberger, Y. Baer, B. Delley, *Phys. Rev. Lett.* **78**(21), 4127 (1997)
25. F. Reinert, D. Ehm, S. Schmidt, G. Nicolay, S. Hüfner, J. Kroha, O. Trovarelli, C. Geibel, *Phys. Rev. Lett.* **87**(10), 106401 (2001)
26. D. Ehm, S. Hüfner, F. Reinert, J. Kroha, P. Wolfle, O. Stockert, C. Geibel, H. v. Lohneysen, *Phys. Rev. B* **76**(4), 045117 (14) (2007), <http://link.aps.org/abstract/PRB/v76/e045117>
27. V. Vildosola, A.M. Llois, M. Alouani, *Phys. Rev. B* **71**(18), 184420 (8) (2005), <http://link.aps.org/abstract/PRB/v71/e184420>
28. O. Sakai, Y. Shimizu, Y. Kaneta, *J. Phys. Soc. Jpn.* **74**(9), 2517 (2005), <http://jpsj.ipap.jp/link?JPSJ/74/2517/>
29. J. Otsuki, Y. Kuramoto, *J. Phys. Soc. Jpn.* **75**, 064707 (2006), (preprint <http://arxiv.org/abs/cond-mat/0602584>), <http://jpsj.ipap.jp/link?JPSJ/75/064707/>
30. P. Roura-Bas, V. Vildosola, L. Manuel, A.M. Llois, *arXiv:0711.4068* (2007), <http://arxiv.org/abs/0711.4068>
31. H. Keiter, J.C. Kimball, *Phys. Rev. Lett.* **25**(10), 672 (1970)
32. N. Grewe, H. Keiter, *Phys. Rev. B* **24**(8), 4420 (1981)
33. P. Coleman, *Phys. Rev. B* **29**(6), 3035 (1984)
34. J. Kroha, P. Wölfle, *J. Phys. Soc. Jpn.* **74**(1), 16 (2005), (preprint at <http://arxiv.org/abs/cond-mat/0410273v2>), <http://arxiv.org/abs/cond-mat/0410273v2>
35. Y. Kuramoto, H. Kojima, *Z. Phys. B* **57**, 95 (1984)
36. N.E. Bickers, D.L. Cox, J.W. Wilkins, *Phys. Rev. B* **36**(4), 2036 (1987)
37. J. Kroha, P. Wölfle, T.A. Costi, *Phys. Rev. Lett.* **79**(2), 261 (1997)
38. F.B. Anders, *J. Phys.: Condens. Matter* **7**, 2801 (1995)

